A hybrid mortar virtual element method for discrete fracture network simulations

A Hybrid Mortar Virtual Element Method For Discrete Fracture Network Simulations[☆]

M. F. Benedetto, S. Berrone*, A. Borio, S. Pieraccini, S. Scialò

Dipartimento di Scienze Matematiche, Politecnico di Torino
Corso Duca degli Abruzzi 24, Torino, 10129, Italy

Abstract

The most challenging issue in performing underground flow simulations in Discrete Fracture Networks (DFN), is to effectively tackle the geometrical difficulties of the problem. In this work we put forward a new application of the Virtual Element Method combined with the Mortar method for domain decomposition: we exploit the flexibility of the VEM in handling polygonal meshes in order to easily construct meshes conforming to the traces on each fracture, and we resort to the mortar approach in order to "weakly" impose continuity of the solution on intersecting fractures. The resulting method replaces the need for matching grids between fractures, so that the meshing process can be performed independently for each fracture. Numerical results show optimal convergence and robustness in handling very complex geometries.

Keywords: Discrete Fracture Networks, Virtual Element Method, Mortar Method, Fracture flows, Darcy flows
2010 MSC: 65N30, 65N50, 68U20, 86-08

1. Introduction

The paper addresses the issue of simulating the state of equilibrium of the hydraulic head of a single–phase fluid flow inside a fractured medium. We consider the rock surrounding the fractures as impervious and model the flow by Darcy's law [1, 2]. The medium is approximated by a Discrete Fracture Network (DFN): fractures are assumed to have a negligible thickness with respect to the other dimensions, and are represented as planar polygons intersecting each

[☆]This research has been partially supported by the Italian MIUR through PRIN research grant 2012HBLYE4_001 *Metodologie innovative nella modellistica differenziale numerica* and by INdAM-GNCS through project *Tecniche numeriche per la simulazione di flussi in reti di fratture di grandi dimensioni* (2015).

*Corresponding author
Email addresses: matias.benedetto@polito.it (M. F. Benedetto), stefano.berrone@polito.it (S. Berrone), andrea.borio@polito.it (A. Borio), sandra.pieraccini@polito.it (S. Pieraccini), stefano.scialo@polito.it (S. Scialò)

other in three dimensional space, with an equivalent bidimensional conductivity obtained by averaging the tridimensional one along the negligible dimension. This setting has been widely studied both from the modeling [1, 3–7] and from the computational point of view [6–14], and it finds its application in the field of evaluation of the properties of a fractured soil, where uncertainty quantification analysis [15, 16] is used to obtain information about the soil, thus requiring a large amount of simulations of the hydraulic head distribution on stochastically generated networks.

When performing such simulations, the main problem to be addressed is the geometrical treatment of the domain, in particular when the global or local conformity of the mesh is required [13, 14, 17].

In some works [12, 18] this difficulty is overcome by modifying the nature of the DFN, notably reducing the number of small angles between the intersections of fractures, which are responsible for the generation of degenerate polygons. This approach, though, changes the global statistical properties of the DFN; this is an issue, in the framework of stochastical analysis.

Recently, efforts have been made towards developing efficient and robust methods that can compute the solution of Darcy's model on arbitrary DFNs. In [8–10, 19] the Finite Element Method and the Extended Finite Element Method have been used for the space discretization on each fracture, while imposing the continuity of the pressure head and the balance of fluxes at intersections in a weak form by means of a PDE-constrained optimization approach: within such framework, the meshing process is completely independent of intersections between fractures.

Other important issues concern the coupling between the DFN and the surrounding rock matrix [11, 20] and more complex models for fracture intersection [21].

In [22, 23] the newly developed Virtual Element Method [24] (VEM) was applied in the DFN framework: the methods proposed therein exploit the flexibility of VEM, that allows the treatment of elements with an arbitrary number of edges, even with flat angles. Thanks to this property, a conforming mesh is easily obtained at a moderate computational cost.

In the present work, the use of VEM in the DFN framework proposed in [22] is coupled with the well established Mortar Method [25]. A major advantage of this new coupling with respect to previous works that also work with a primal formulation of the problem is that the flux entering/exiting each fracture from its intersections is directly obtained as part of the solution of the discrete problem and not through a post-processing of the results.

The paper is organized as follows: in Section 2 we state the problem setting; in Section 3 we briefly recall the main features of the VEM needed for the description of our method; Section 4 is devoted to the description of the hybrid method obtained from coupling the VEM with the mortar method; Section 5 addresses some implementation issues related to the generation of the locally conforming mesh; finally, Section 6 reports some numerical results assessing the behaviour of the method.

2. Problem formulation

A DFN, Ω, is a set of N open planar polygons F_i, $i = 1, \dots, N$, representing the fractures in the medium. In the sequel, we will identify the fractures with the polygons. Fractures intersect each other along segments called *traces*. We assume throughout the paper that traces are given by the intersection of exactly two fractures. Whenever two traces intersect each other, we split both traces into two sub-traces. The set of all traces and sub-traces will be denoted by $\mathcal{S}$. For the sake of simplicity, in the sequel we will refer to all elements in $\mathcal{S}$ as traces. For each $S \in \mathcal{S}$, it is convenient to identify the set $\mathcal{I}_S = \{i, j\}$ of the indices of the two fractures intersecting at S. For any function or set defined on the whole DFN, its restriction to fracture F_i will be denoted using the subscript i.

On the domain Ω, we consider the Darcy's law as a model for the equilibrium of the hydraulic head $H = P + \zeta$, where $P = p/(\rho\, g)$ is the fluid pressure, g is the gravitational constant, ρ the fluid density and ζ its elevation. We introduce on each fracture the transmissivity K_i, which is assumed, for the sake of simplicity, to be a scalar function of the local tangential coordinates system on F_i. Let Γ^D be a non-empty portion of $\partial\Omega$ on which the Dirichlet boundary condition H^D is imposed, and let us set $\Gamma_i^D = \Gamma^D \cap F_i$. Note that Γ_i^D is allowed to be empty for some i. Let us assume that $H_i^D \in \mathrm{H}^{\frac{1}{2}}(\Gamma_i^D)$ for all $i \in \{1, \dots, N\}$. Furthermore, let $\Gamma_i^N = \partial F_i \setminus \Gamma_i^D$ be the local Neumann boundary and let $H_i^N \in \mathrm{H}^{-\frac{1}{2}}(\Gamma_i^N)$ be the Neumann boundary condition imposed therein.

Let us define the following functional spaces:

$$
\begin{aligned}
V_i &= \left\{ v \in \mathrm{H}^1(F_i) \colon\ \gamma_{\Gamma_i^D}(v) = 0 \right\} \quad \forall i = 1, \dots, N\,, \\
V_i^D &= \left\{ v \in \mathrm{H}^1(F_i) \colon\ \gamma_{\Gamma_i^D}(v) = H_i^D \right\} \quad \forall i = 1, \dots, N\,, \\
V^D &= \prod_{i=1}^N V_i^D\,, \qquad V = \prod_{i=1}^N V_i\,,
\end{aligned}
$$

where $\gamma_{\Gamma_i^D} : \mathrm{H}^1(F_i) \mapsto \mathrm{H}^{\frac{1}{2}}(\Gamma_i^D)$ is the trace operator on Γ_i^D.

The problem of interest is to find $H \in V^D$ such that $H = H_0 + R^D$ where $R_i^D = R^D\big|_{F_i}$ is a lifting of H_i^D on $\mathrm{H}^1(F_i)$ and $H_0 \in V$ satisfies, for any given $v \in V$ and any $i = 1, \dots, N$,

$$
\begin{aligned}
(K_i \nabla H_{0,i}, \nabla v_i)_{F_i} - \sum_{S \in \mathcal{S}} \left\langle \left[\!\left[K_i \frac{\partial H_i}{\partial \mathbf{n}_S^i} \right]\!\right]_S, v_i \right\rangle_{\pm\frac{1}{2}, S} &= (f_i, v_i)_{F_i} + \left\langle H_i^N, v_i \right\rangle_{\pm\frac{1}{2}, \Gamma_i^N} \\
&\quad - \left(K_i \nabla R_i^D, \nabla v_i\right)_{F_i} \qquad (1)
\end{aligned}
$$

where $\langle \cdot, \cdot \rangle_{\pm\alpha,\omega}$ is the duality product between $\mathrm{H}^{-\alpha}(\omega)$ and $\mathrm{H}^{\alpha}(\omega)$, $\mathbf{n}_S^i$ is the unit vector normal to trace S on fracture F_i, and the symbol $\left[\!\left[K_i \frac{\partial H_i}{\partial \mathbf{n}_S^i} \right]\!\right]_S$ denotes the jump of the co-normal derivative of H_i across S on F_i. The equations on

each fracture are coupled by the balance of fluxes on traces:

$$\forall S \in \mathcal{S}, \text{ if } \mathcal{I}_S = \{i,j\}, \quad \left[\!\left[K_i \frac{\partial H_i}{\partial \mathbf{n}_S^i} \right]\!\right]_S + \left[\!\left[K_j \frac{\partial H_j}{\partial \mathbf{n}_S^j} \right]\!\right]_S = 0\,, \tag{2}$$

and by the continuity of the solution across traces, that can be written as:

$$\forall S \in \mathcal{S}, \forall \psi \in \mathrm{H}^{-\frac{1}{2}}(S) = \left(\mathrm{H}_{00}^{\frac{1}{2}}(S)\right)', \langle [\![H]\!]_S, \psi \rangle_{\pm\frac{1}{2},S} = 0\,. \tag{3}$$

We introduce

$$\forall S \in \mathcal{S}, \forall \psi \in \mathrm{H}^{-\frac{1}{2}}(S), \quad b_S(v,\psi) = \langle [\![v]\!]_S, \psi \rangle_{\pm\frac{1}{2},S}\,, \tag{4}$$

and rewrite (3) as

$$\forall S \in \mathcal{S}, \forall \psi \in \mathrm{H}^{-\frac{1}{2}}(S), \quad b_S(H,\psi) = 0\,. \tag{5}$$

For the sake of convenience in rewriting the jump of a function on a trace S, let us fix the following sign convention: for each $S \in \mathcal{S}$, with $\mathcal{I}_S = \{i,j\}$, let us introduce the function $m_S : \mathcal{I}_S \to \{0,1\}$ as follows:

$$m_S(k) = \begin{cases} 1 & \text{if} \quad k = \min\{i,j\} \\ 0 & \text{otherwhise} \end{cases}.$$

Hence, we may write

$$\forall v \in V, \forall S \in \mathcal{S}, \, [\![v]\!]_S = \sum_{i \in \mathcal{I}_S} (-1)^{m_S(i)} \, \gamma_s(v_i)\,. \tag{6}$$

We introduce the space $M = \prod_{S\in\mathcal{S}} \mathrm{H}^{-\frac{1}{2}}(S)$ and set

$$\forall v_i \in V_i, \forall \psi \in M, \quad b_i(v_i,\psi) = \sum_{S \in \mathcal{S}_i} (-1)^{m_S(i)} \langle \gamma_s(v_i), \psi_S \rangle_{\pm\frac{1}{2},S}\,. \tag{7}$$

With these definitions at hand, we define $\Lambda \in M$ such that, $\forall S \in \mathcal{S}$,

$$\Lambda_S = \left[\!\left[K_i \frac{\partial H_i}{\partial \mathbf{n}_S^i} \right]\!\right]_S,$$

where i is such that $m_S(i) = 1$. Then, defining $a_i : V_i \times V_i \mapsto \mathbb{R}$ as

$$a_i(u_i,v_i) = (K_i \nabla u_i, \nabla v_i)_{F_i} \quad \forall i = 1,\ldots,N\,, \tag{8}$$

equation (1) can be written as

$$a_i(H_{0i},v_i) + b_i(v_i,\Lambda) = (f_i,v_i)_{F_i} + \left\langle H_i^N, v_i \right\rangle_{\pm\frac{1}{2},\Gamma_i^N} - a_i\left(R_i^D, v_i\right) \quad \forall v \in V\,. \tag{9}$$

In view of a global formulation of the problem, we define

$$a\left(u,v\right)=\sum_{i=1}^{N}a_i\left(u_i,v_i\right)\quad\forall u,v\in V\,,\tag{10}$$

$$b\left(v,\psi\right)=\sum_{i=1}^{N}b_i\left(v_i,\psi\right)\quad\forall v\in V,\,\psi\in M\,.\tag{11}$$

Note that due to (4), (7) and (5) we have $b\left(H,\psi\right)=\sum_{S\in\mathcal{S}}b_S\left(H,\psi\right)=0$. Summing up (9) over all the fractures we obtain:

$$\begin{cases}a\left(H_0,v\right)+b\left(v,\Lambda\right)=\left(f,v\right)+\left\langle H^N,v\right\rangle_{\pm\frac{1}{2},\Gamma^N}-a\left(R^D,v\right) & \forall v\in V,\\ b\left(H_0,\psi\right)=-b\left(R^D,\psi\right) & \forall\psi\in M.\end{cases}\tag{12}$$

Let us endow V^D and V with the norm

$$\|\,v\,\|_V=\left(\sum_{i=1}^{N}\|\,v_i\,\|^2_{\mathrm{L}^2(F_i)}+a_i\left(v_i,v_i\right)\right)^{\frac{1}{2}}.\tag{13}$$

Well-posedness of problem (12) follows observing that, introducing the Hilbert space

$$W=\left\{v\in V\colon\forall S\in\mathcal{S},\,\forall\psi\in\mathrm{H}^{-\frac{1}{2}}(S),\,\left\langle[\![v]\!]_S\,,\psi\right\rangle_{\pm\frac{1}{2},S}=0\right\}=\ker(b)\,,$$

problem (12) is equivalent to: *find* $H_0\in W$ *such that*

$$a\left(H_0,v\right)=\left(f,v\right)+\left\langle H^N,v\right\rangle_{\pm\frac{1}{2},\Gamma^N}-a\left(R^D,v\right)\quad\forall v\in W\,.$$

3. The Virtual Element Method

In this section we briefly recall the main features of the conforming VEM which are useful for the description of the approach proposed in the following sections. The reader is referred to the seminal papers [24, 26] for a thorough description and to [27–31] for further developments of the method.

The VEM is a generalization of the standard finite element method to polygonal meshes, and it includes some of the ideas present in the mimetic difference method [32, 33]. The peculiarity of the method is that the discrete functional space contains more general functions in addition to standard piecewise polynomials, namely, it contains functions whose restrictions to element edges are polynomials, whereas in the interior only information of the function for certain degrees of freedom is known. When computing the stiffness matrix or the right hand side of the problem, the integrals will be computed exactly only if at least one of the two factors is a polynomial, whereas in other cases they will be substituted by operations on the degrees of freedom suitably defined to maintain the right order of convergence.

Let us consider a given fracture $F_i \subset \mathbb{R}^2$, a mesh $\tau_{\delta,i}$ on F_i with mesh parameter δ, representing the maximum element size, and consisting of a finite number of polygons E, convex in the following, with an arbitrary number of edges. We denote by k the desired order of accuracy of the method and by $\mathbb{P}_k$ the space of the polynomials of maximum order k, with $\mathbb{P}_{-1} = \{0\}$. The local virtual element space $V_{k,\delta}(E)$ is defined as

$$V_{k,\delta}(E) = \big\{ v_\delta \in \mathrm{H}^1(E) : v_{\delta|\partial E} \in C^0(\partial E),\, v_{\delta|e} \in \mathbb{P}_k(e),\, \forall e \subset \partial E, \\ \Delta v_\delta \in \mathbb{P}_{k-2}(E) \}$$

where ∂E is the boundary of E, and e is an edge. Note that from the definition it clearly follows that $\mathbb{P}_k(E) \subseteq V_{k,\delta}(E)$; the latter set may also include other non-polynomial functions.

Following [24], for each element E the following set of DOFs is introduced:

- the value of v_δ at the vertices of E;
- the value of v_δ at $k-1$ internal points on each edge of E;
- the scaled moments $\frac{1}{|E|}\int_E v_\delta m_\alpha$ for $|\alpha| \leq k-2$,

where m_α, with $\alpha = (\alpha_1, \alpha_2)$, denotes the scaled monomial

$$m_\alpha(x,y) = \left(\frac{x - x_c}{h_E}\right)^{\alpha_1} \left(\frac{y - y_c}{h_E}\right)^{\alpha_2},$$

being (x_c, y_c) and h_E the centroid and the diameter of the element E, respectively. Edge moments can also be chosen as degrees of freedom instead of internal edge point values; in general, any set of DOFs that completely defines $v_{\delta|e}$ for all edges of the element is a valid choice. Note that for $k = 1$ the set of DOFs is given by the values of v_δ at the vertices of E. The selected set of degrees of freedom is unisolvent [24] and therefore, given an element E with n_v vertices, we have that the dimension of $V_{k,\delta}(E)$ is

$$\dim V_{k,\delta}(E) = n_v k + k(k-1)/2\,.$$

We can define basis functions ϕ_ℓ with $\ell = 1, ..., \dim V_{k,\delta}(E)$ in $V_{k,\delta}(E)$ in such a way that $\mathrm{dof}_\ell(\phi_m) = \delta_{\ell m}$ where $\mathrm{dof}_\ell(v) :=$ *value of* v *at* ℓ*-th degree of freedom.* The global virtual element space on F_i is:

$$V_{k,\delta}(F_i) = \{ v_\delta \colon v_\delta|_E \in V_{k,\delta}(E) \text{ for all } E \in \tau_{\delta,i} \} \subset \mathrm{H}^1(F_i)\ .$$

Inclusion in $\mathrm{H}^1(F_i)$ is a consequence of the choice of edges and vertices as DOFs, that guarantees continuity of any function $v_\delta \in V_{k,\delta}(F_i)$ on internal edges of the mesh.

Let us assume for the sake of simplicity that the fracture transmissivity K_i, $i = 1, \ldots, N$, is constant on F_i, and let us introduce, on each element E of F_i, the bilinear form

$$a^E(u,v) = K_i(\nabla u, \nabla v)_E \quad \forall u, v \in V_{k,\delta}(E)\,.$$

For $k \geq 1$, let us introduce a projection operator on E:

$$\Pi^{\nabla}_{E,k} : V_{k,\delta}(E) \longrightarrow \mathbb{P}_k(E)\,,$$

defined by

$$\int_E \nabla p_k \cdot (\nabla v_\delta - \nabla \Pi^{\nabla}_{E,k} v_\delta) = 0 \quad \forall p_k \in \mathbb{P}_k(E)\,, \tag{14}$$

$$\begin{cases} \displaystyle\int_E \Pi^{\nabla}_{E,k} v_\delta = \int_E v_\delta & k > 1, \\ \displaystyle\sum_{i=1}^{n_v} \Pi^{\nabla}_{E,k} v_\delta(\mathcal{V}_i) = \sum_{i=1}^{n_v} v_\delta(\mathcal{V}_i) & k = 1, \end{cases} \tag{15}$$

where $\mathcal{V}_i$ are the vertices of the element.

Note that

$$\Pi^{\nabla}_{E,k} p_k = p_k \text{ for all } p_k \in \mathbb{P}_k(E)\,.$$

The projection represents an orthogonality condition in the scalar product induced by the bilinear form a. Thanks to integration by parts, the computation of $\Pi^{\nabla}_{E,k} v_\delta$ can be performed just by exploiting the knowledge of v_δ in the degrees of freedom [26]. Equation (14) completely determines the gradient of the projection, while (15) takes care of the constant part. Other options for (15) exist [24, 31].

Remark 3.1. The assumption of K_i being constant on each fracture is made here for the ease of description. In case of problems presenting non-constant coefficients or a more general second order differential equation including lower order terms, other projectors have to be used in order to retain optimal convergence [31].

Let us now introduce the discrete bilinear form on the element E as:

$$\begin{aligned} a^E_\delta(u_\delta, v_\delta) = {} & a^E\left(\Pi^{\nabla}_{E,k} u_\delta, \Pi^{\nabla}_{E,k} v_\delta\right) \\ & + S^E_\delta\left(u_\delta - \Pi^{\nabla}_{E,k} u_\delta, v_\delta - \Pi^{\nabla}_{E,k} v_\delta\right), \quad \forall u_\delta, v_\delta \in V_{k,\delta}(E)\,, \end{aligned} \tag{16}$$

where S^E_δ is any symmetric, positive definite bilinear form that verifies

$$C_0 a^E(v_\delta, v_\delta) \leq S^E_\delta(v_\delta, v_\delta) \leq C_1 a^E(v_\delta, v_\delta) \quad \forall v_\delta \in \ker(\Pi^{\nabla}_{E,k})\,,$$

for constants $C_0, C_1 > 0$ independent of E. This means that $S^E_\delta(v, v)$ scales like $a^E(v, v)$ on the kernel of $\Pi^{\nabla}_{E,k}$. A possible choice for S^E_δ is the Euclidean product in $\mathbb{R}^{\#V^E_{k,\delta} \times \#V^E_{k,\delta}}$ between vectors whose components are the values of the functions at the degrees of freedom. Note that the first term of (16) ensures the consistency of the form, and the second one has in charge its stability. In particular, we have

$$a^E_\delta(v_\delta, p_k) = a^E(v_\delta, p_k) \quad \forall v_\delta \in V_\delta,\, \forall p_k \in \mathbb{P}_k(E)\,. \tag{17}$$

Going back to the whole DFN, the global discrete bilinear form is defined as

$$a_\delta(h_\delta, v_\delta) = \sum_{i=1}^{N} \sum_{E \in \tau_{\delta,i}} a_\delta^E(h_\delta, v_\delta) \quad \forall h_\delta, v_\delta \in V_{k,\delta} = \prod_{i=1}^{N} V_{k,\delta}(F_i)\,. \tag{18}$$

Under proper regularity assumptions, it can be proved [24] that a_δ is equivalent to a, i.e. that there exist two positive constants α^* and α_*, independent of δ and N, such that

$$\alpha_*\, a\,(v_\delta, v_\delta) \le a_\delta\,(v_\delta, v_\delta) \le \alpha^*\, a\,(v_\delta, v_\delta) \quad \forall v_\delta \in V_{k,\delta}\,. \tag{19}$$

For the right hand side with load term f, it is enough for optimal convergence [26] to consider the following discrete scalar products:

$$(f, v_\delta)_\delta = \sum_{E \in \tau_\delta} \int_E f \Pi^0_{E,k} v_\delta \tag{20}$$

where $\forall E \in \mathcal{T}_h$, $\Pi^0_{E,k}$ is computed as in [26, Sections 5.3–6.1], i.e. it is the polynomial function such that, $\forall v \in V_{k,\delta}(E)$,

$$\begin{aligned} \left(\Pi^0_{E,k} v, p\right)_E &= (v, p)_E \quad \forall p \in \mathbb{P}_{k-2}\,(E)\,, \\ \left(\Pi^0_{E,k} v, p\right)_E &= \left(\Pi^\nabla_{E,k} v, p\right)_E \quad \forall p \in \mathbb{P}_k\,(E) \setminus \mathbb{P}_{k-2}\,(E)\,. \end{aligned}$$

4. Mortar formulation of the problem

In this section we introduce a Mortar formulation for problem (12), in conjunction with the VEM for the finite dimensional approximation of V.

From now on, let us consider the VEM of order k and let us introduce the spaces

$$V_\delta = \left\{ v_\delta \in V_{k,\delta} \colon\ \gamma_{\Gamma_i^D}(v_\delta) = 0 \quad \forall i = 1, \dots, N \right\}, \tag{21}$$

$$V_\delta^D = \left\{ v_\delta \in V_{k,\delta} \colon\ \gamma_{\Gamma_i^D}(v_\delta) = \Pi^0_{k,\Gamma^D}(H^D) \quad \forall i = 1, \dots, N \right\}, \tag{22}$$

where Π^0_{k,Γ^D} is the piecewise $\mathrm{L}^2(e)$ projection on polynomials of degree $\le k$ for all edges e such that $e \cap \Gamma^D \neq \emptyset$. We equip both spaces with the same norm as V. The Mortar Method [25] consists in weakening the continuity of the solution on each trace $S \in \mathcal{S}$, replacing it by suitable orthogonality conditions with respect to a proper finite dimensional subspace of $\mathrm{H}^{-\frac{1}{2}}(S)$, which will be denoted by $M_{\delta,S} \subset \mathrm{L}^2(S)$. Going back to equation (9), let h and λ denote the discrete counterpart of H and Λ, respectively; the discrete version of (9) is written as: find $h \in V_\delta^D$ such that, for $i = 1, \dots, N$

$$a_{\delta i}\,(h_i, v_{\delta i}) + b_i\,(v_{\delta i}, \lambda) = (f_i, v_{\delta i})_\delta + \left(H^N, v_{\delta i}\right)_{\Gamma_i^N} \quad \forall v_\delta \in V_\delta\,. \tag{23}$$

Following the mortar terminology, for each $S \in \mathcal{S}$, $S = \bar{F}_i \cap \bar{F}_j$, we call *mortar fracture* the one whose index i is such that $m_S(i) = 0$, while the other fracture

intersecting at S will be denoted as *non-mortar*. In the present context, $\lambda_S = \lambda|_S$ will approximate the jump of the co-normal derivative of the solution on the non-mortar fracture, while the jump on the mortar fracture will be approximated by $-\lambda_S$.

Considering again a lifting R_δ^D of $\Pi^0_{k,\Gamma^D}(H^D)$ and summing up (23) over all fractures, the global form a_δ defined by (18) arises and the problem can be rewritten as: find $h = h_0 + R_\delta^D$, with $h_0 \in V_\delta$, and $\lambda \in M_\delta$ such that

$$\begin{cases} a_\delta\left(h_0, v_\delta\right) + b\left(v_\delta, \lambda\right) = \left(f, v_\delta\right)_\delta + \left(H^N, v_\delta\right)_{\Gamma^N} - a_\delta\left(R_\delta^D, v_\delta\right) & \forall v_\delta \in V_\delta, \\ b\left(h_0, \psi_\delta\right) = -b\left(R_\delta^D, \psi_\delta\right) & \forall \psi_\delta \in M_\delta, \end{cases} \tag{24}$$

being

$$M_\delta = \prod_{S \in \mathcal{S}} M_{\delta,S}, \tag{25}$$

and $b(v_\delta, \psi_\delta)$ computed as an integral in $\mathrm{L}^2(S)$.

4.1. Well-posedness of the discrete problem

Following [34, Corollary 2.1], the well-posedness of problem (24) is guaranteed if a_δ is coercive on

$$W_\delta = \left\{ v_\delta \in V_\delta \colon b(v_\delta, \psi_\delta) = 0 \quad \forall \psi_\delta \in M_\delta \right\}, \tag{26}$$

and an *inf-sup* condition holds:

$$\exists \beta > 0 \colon \inf_{\psi_\delta \in M_\delta} \sup_{v_\delta \in V_\delta} \frac{b\left(v_\delta, \psi_\delta\right)}{\| v_\delta \|_V \| \psi_\delta \|_M} \geq \beta\,. \tag{27}$$

The existence of a constant β independent of δ satisfying (27) was proved in [35] making use of [36, Lemma 10] in the case of a polynomial Finite Element approximation on a regular triangulation. The same proof applies here under the following assumption.

Assumption 1. *There exists a constant $\sigma > 0$ independent of δ such that, for each $E \in \tau_{\delta,i}$, for $i = 1, \ldots, N$, the distance between any two vertices of E is larger then or equal to σh_E, where h_E is the diameter of E.*

Under this assumption, consider a trace S and a segment e belonging to the discretization of S. Let E be one of the two polygons sharing e. By Assumption 1, we can construct in the interior of E a triangle $T_{e,E}$ having e as one of its edges and having a shape regularity which depends uniquely on σ (for example, for convex elements, by connecting the extrema of e with the barycenter of E). The area of such a triangle scales as the area of E divided by the number of edges of E. We are thus led to make the following assumption.

Assumption 2. *The number of edges of the elements of τ_δ is limited independently of δ.*

With this last assumption, the area of $T_{e,E}$ scales like the area of E and thus, the norm of any function belonging to the finite dimensional space on $T_{e,E}$ is equivalent to the one on E. From [36, Lemma 10], we obtain the existence of an inf-sup constant independent of δ for $T_{e,E}$ and thus prove the existence of such a constant for E by the equivalence of the norms.

To prove the coercivity of a_δ on W_δ, we first prove the coercivity of a on such space and then use the equivalence (19). The key result needed is the following.

Proposition 4.1. *Assume that M_δ contains the functions which are constant on each trace. Then, the functional $v_\delta \mapsto |\!|\!| v_\delta |\!|\!|$ is a norm over W_δ.*

Proof. It is enough to verify that $|\!|\!| v_\delta |\!|\!| = 0$ only if $v_\delta = 0$. Let $v_\delta \in W_\delta$ be such that $|\!|\!| v_\delta |\!|\!| = 0$. Then it must be constant on each fracture, since its gradient on each fracture is null. Furthermore, v_δ clearly vanishes on all fractures such that $\Gamma_i^D \neq \emptyset$. It is now easy to prove that v_δ vanishes on all fractures. Indeed, let S be a trace shared by fractures F_i and F_j, with $\gamma_S(v_{\delta i}) = 0$; thanks to the mortar condition one has

$$(\llbracket v_\delta \rrbracket_S, 1)_S = |S| \llbracket v_\delta \rrbracket_S = 0 \Rightarrow \gamma_S(v_{\delta j}) = \gamma_S(v_{\delta i}) = 0$$

and since $v_{\delta i}$ and $v_{\delta j}$ are constant, it follows that $v_{\delta j} = 0$. Thanks to the network connectivity, this ensures that v_δ vanishes on all the fractures. □

From now on, M_δ is required to satisfy the assumption of Proposition 4.1. It follows that a is coercive with coercivity constant 1 on W_δ. By (19), a_δ is coercive with coercivity constant α_*.

4.2. A priori error estimates

We are now able to derive an *a priori* error estimate. To this aim, we introduce the operators $\mathscr{F}, \mathscr{F}_\delta \in V'$ defined such that

$$\langle \mathscr{F}, v \rangle_{\pm 1,\Omega} = (f, v)_\Omega, \qquad \langle \mathscr{F}_\delta, v \rangle_{\pm 1,\Omega} = (f, v)_\delta.$$

Furthermore, define

$$W_\delta^D = \left\{ v \in V_\delta^D \colon b(v, \psi) = 0, \quad \forall \psi \in M_\delta \right\}, \tag{28}$$

$$\mathbb{P}_k^D(\Omega) = \left\{ p \in V_\delta^D : \, p \in \mathbb{P}_k(E), \quad \forall E \in \tau_\delta \right\}. \tag{29}$$

The main result concerning the a priori error estimate is stated in the following Theorem. The proof is reported in Appendix A.

Theorem 4.1. *Let V_δ, M_δ, W_δ, W_δ^D and $\mathbb{P}_k^D(\Omega)$ be defined as in* (21), (25), (26), (28) *and* (29)*, respectively. Then, the solution (h, λ) to problem* (24) *and the solution (H, Λ) to problem* (9) *satisfy*

$$\begin{aligned} |\!|\!| H - h |\!|\!| \leq \left(1 + \frac{\alpha^*}{\alpha_*}\right) \inf_{v_\delta \in W_\delta^D} |\!|\!| H - v_\delta |\!|\!| + \frac{1 + \alpha^*}{\alpha_*} \inf_{p_k \in \mathbb{P}_k^D(\Omega)} |\!|\!| H - p_k |\!|\!| \\ + \frac{1}{\alpha_*} \left(\inf_{\psi_\delta \in M_\delta} \sup_{v_\delta \in W_\delta} \frac{b(v_\delta, \Lambda - \psi_\delta)}{|\!|\!| v_\delta |\!|\!|} \right) + \frac{1 + C_\Omega}{\alpha_*} \| \mathscr{F} - \mathscr{F}_\delta \|_{V'}. \end{aligned} \tag{30}$$

Moreover, assume (27) *is satisfied. Then,*

$$\begin{aligned} \| \Lambda - \lambda \|_M \leq \left(1 + \frac{1}{\beta}\right) \inf_{\psi_\delta \in M_\delta} \| \Lambda - \psi_\delta \|_M + \frac{\sqrt{\alpha^*}}{\beta} \| H - h \| \\ + \frac{1 + \sqrt{\alpha^*}}{\beta} \inf_{p_k \in \mathbb{P}_k^D(\Omega)} \| H - p_k \| + \frac{1}{\beta} \| \mathscr{F} - \mathscr{F}_\delta \|_{V'} \ . \end{aligned} \tag{31}$$

5. Implementation

We describe in this section some details concerning the practical implementation of the method.

5.1. Mesh generation and trace management

Following closely the ideas in [22], we start by independently introducing a good quality triangular mesh on each fracture, disregarding trace positions. Such triangulation will be called *base mesh*. On each fracture, the base mesh is then modified in such a way that a new polygonal mesh is obtained, that is locally conforming to the traces of the fractures. This means that traces will be covered by edges of the new polygonal elements, though we remark that elements on meshes from different fractures induce a different discretization of the same trace. This new mesh will be suitable for the application of the method described in the previous sections and it will be called *VEM mesh*. The procedure for obtaining the VEM mesh is the following. Whenever a trace intersects an edge of the triangulation, a new node is created at the intersection. Each trace tip defines a new node and the trace segment is prolonged up to the nearest edge of the triangulation, thereby creating a new edge and a new node. When two traces intersect each other, they are split into two sub-traces and in their intersection a new node is created. Whenever an element of the mesh is cut by a (possibly prolonged) trace segment, it is split into two parts which become new elements of the polygonal mesh in their own right. Finally, traces without internal nodes receive the addition of a new node in its midpoint, which is necessary to define the discrete Mortar space for the trace. The overall procedure thus results in a polygonal mesh whose elements are convex polygons made of an arbitrary number of edges.

Figure 1 is illustrative for such procedure. Focusing on a single fracture, we depict on the left the base mesh introduced, and the local traces present on the fracture, denoted by LT and with a fracture-local numbering from 1 to 15. On the right, the VEM mesh obtained is represented. Note that new traces are introduced by splitting the original traces into sub-traces. Note, as well, the generation of new nodes and elements obtained via trace segment prolongation and the addition of one internal node (see, e.g., the original local trace 3 on the top of the fracture). To better highlight the number of edges in the elements, a different coloring is used for elements with a different number of edges.

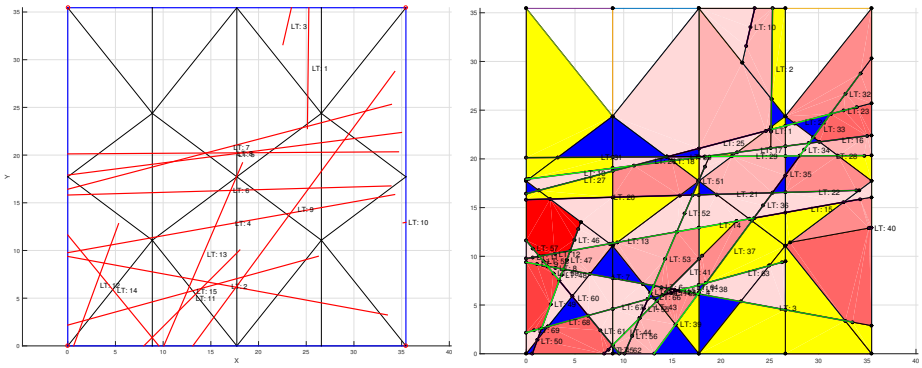

Figure 1: Mesh examples. Left: base mesh; right: VEM mesh.

Remark 5.1. In order to verify Assumption 1, a mesh smoothing process can be designed, in order to improve the quality of the VEM mesh, reduce the number of DOFs and prevent irregular elements in the discretization. Let us introduce for each vertex a quantity r_{m} called *moving radius*, defined as a fixed rate of the smallest edge connected to that vertex. Correspondingly, we define a *moving ball* as a ball with center the vertex and radius r_{m}. Then:

1. if a trace tip lies within a moving ball of a vertex, the vertex is moved on the tip (see Figure 2a);
2. if the intersection between two traces is within the moving ball of a vertex not previously moved to a tip, the latter is moved on the intersection (see Figure 2b);
3. if a vertex not previously moved is closer to a trace than the moving radius, it is moved orthogonally onto the trace (see Figure 2c).

This procedure does not cover the case in which two traces intersect each other with a very small angle or very small traces, but from the numerical results (see, in particular, Section 6.2) we can say that the method is sufficiently robust to deal with this kind of issues.

Remark 5.2. Assumption 2 is satisfied by the VEM mesh. Indeed, the triangles of the base mesh are only split when a trace cuts them. Thus, the number of edges of the new polygonal elements is limited by the number of traces cutting the element (that is bounded by the number of traces on the fracture), plus 3.

5.2. Matrix Formulation of the problem

On the discretization of S induced by the triangulation on the non-mortar fracture, we introduce a finite dimensional subspace of dimension N_S, containing the constant functions (this is required for well-posedness, see Proposition 4.1). Let N_h and N_λ be the total number of degrees of freedom for h and λ, respectively, and set $N_{\mathrm{dof}} = N_h + N_\lambda$; let us denote by ϕ_k, $k = 1, \ldots, N_h$, and

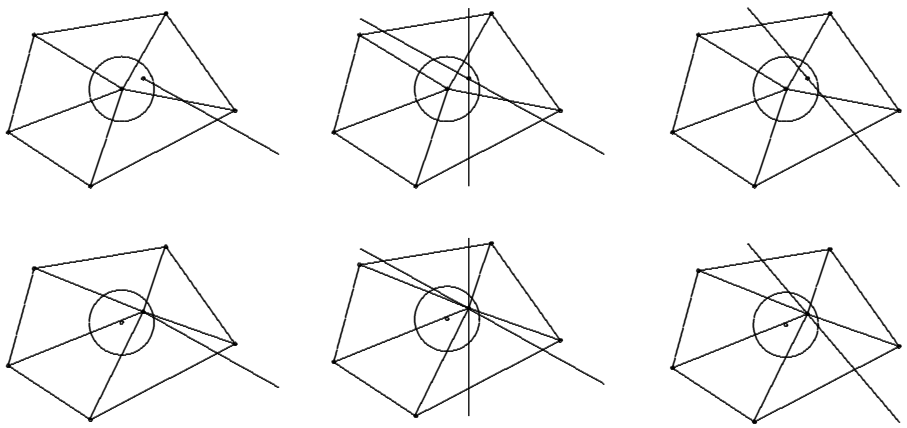

(a) (b) (c)

Figure 2: Mesh smoothing process. Top: before mesh smoothing; bottom: after mesh smoothing. Cases: (a) trace tip close to a vertex; (b) traces intersecting close to a vertex; (c) trace very close to a vertex.

ψ_l, $l = 1, \ldots, N_\lambda$, the basis functions for h and λ, respectively. Finally, let N^D be the number of basis functions ϕ_j^D used to define the lifting R^D of the Dirichlet boundary condition. Then, problem (24) can be written as

$$\sum_{j=1}^{N_h} a_\delta\left(\phi_j, \phi_k\right) h_j + \sum_{l=1}^{N_\lambda} b\left(\phi_k, \psi_l\right) \lambda_l = \left(f, \phi_k\right)_\delta + \left(H^N, \phi_k\right)_{\Gamma^N} - \sum_{j=1}^{N_D} a_\delta\left(\phi_j^D, \phi_k\right) h_j^D$$

$$\sum_{j=1}^{N_h} b\left(\phi_j, \psi_m\right) h_j = -\sum_{j=1}^{N_D} b\left(\phi_j^D, \psi_m\right) h_j^D$$

$\forall k = 1, \ldots, N_h$ and $\forall m = 1, \ldots, N_\lambda$, where h_j^D is the value of $\Pi^0_{k,\Gamma^D}(H^D)$ at the boundary node corresponding to ϕ_j^D. Summarizing, we have to solve the system

$$\begin{pmatrix} A \in \mathbb{R}^{N_h, N_h} & B \in \mathbb{R}^{N_h, N_\lambda} \\ B^\intercal \in \mathbb{R}^{N_\lambda, N_h} & O \in \mathbb{R}^{N_\lambda, N_\lambda} \end{pmatrix} \begin{pmatrix} \mathbf{h} \\ \boldsymbol{\lambda} \end{pmatrix} = \begin{pmatrix} \mathbf{F} \\ \boldsymbol{\Psi} \end{pmatrix}, \tag{32}$$

where

$$A_{kj} = a_\delta\left(\phi_k, \phi_j\right), \qquad B_{jl} = b\left(\phi_j, \psi_l\right)$$

$$F_k = \left(f, \phi_k\right)_\delta + \left(H^N, \phi_k\right)_{\Gamma^N} - \sum_{j=1}^{N_D} a_\delta\left(\phi_j^D, \phi_k\right) h_j^D, \quad \Psi_m = -\sum_{j=1}^{N_D} b\left(\phi_j^D, \psi_m\right) h_j^D.$$

For the practical construction of the VEM stiffness matrix and right hand side vector, we refer the reader to [26]. We remark that the construction of the matrix B can be done by standard quadrature formulas, since the analytical expression of the basis functions on the edges of each element is known.

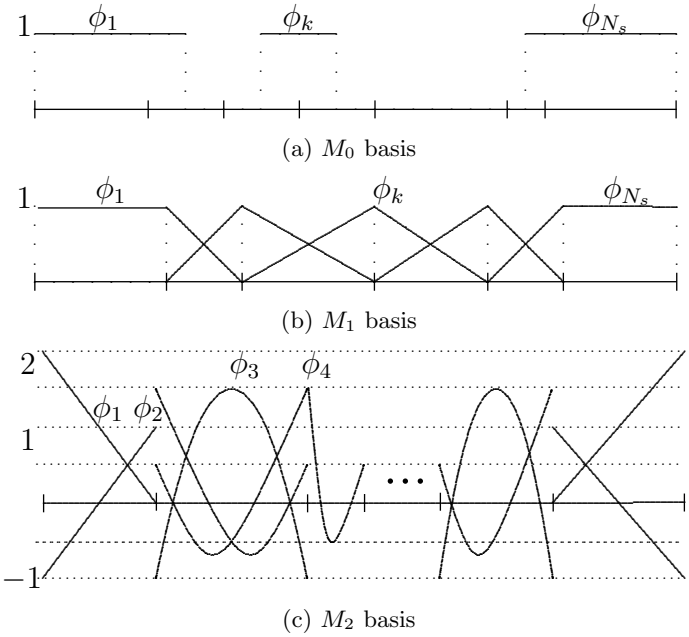

(a) M_0 basis

(b) M_1 basis

(c) M_2 basis

Figure 3: Lagrange multiplier basis

5.3. Bases for the discrete Lagrange multipliers

In this subsection we give details about the choice adopted for the space $M_{\delta,S}$, for each $S \in \mathcal{S}$. For a thorough description of the possible choices of Mortar bases, we refer the reader to [37].

In this work we have used three bases: the basis M_0, composed by piecewise constant functions; the basis M_1, given by continuous piecewise linear functions, except for the first and last intervals on which the functions are taken constant; the basis M_2, given by discontinuous piecewise quadratic functions, except for the first and last interval where the functions are linear. These bases are depicted in Figure 3.

6. Numerical results

We present in this section some numerical results aimed at assessing the practical behavior of the method. The results are obtained on two classes of problems: firstly, we present a benchmark problem for which the exact solution is known, with some convergence results; secondly, we analyse the performance of the method on larger DFNs that introduce several geometrical complexities. All the numerical results here reported are obtained without any kind of mesh smoothing (see Remark 5.1), in order to test the robustness of the method.

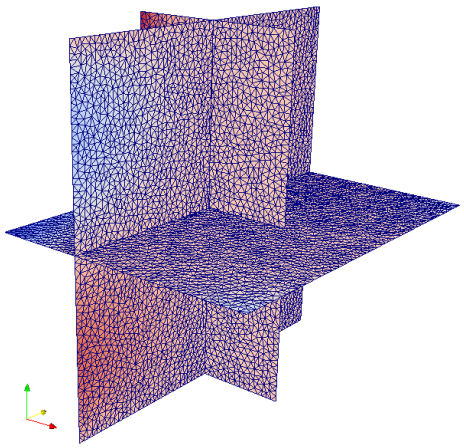

Figure 4: Benchmark problem: geometry of the network

6.1. Benchmark problem

The benchmark DFN consists of 3 fractures as shown in Figure 4. Despite being a simple network, it presents two geometrical features (a trace intersection and a trace tip) which make it worthwhile to analyse the behavior of the method at tackling them. The computational domain $\Omega = F_1 \cup F_2 \cup F_3$ is defined by

$$\begin{aligned}
F_1 &= \left\{(x,y,z) \in \mathbb{R}^3 : -1 \le x \le 1/2,\ -1 \le y \le 1,\ z = 0\right\}, \\
F_2 &= \left\{(x,y,z) \in \mathbb{R}^3 : -1 \le x \le 0,\ y = 0,\ -1 \le z \le 1\right\}, \\
F_3 &= \left\{(x,y,z) \in \mathbb{R}^3 : x = -1/2,\ -1 \le y \le 1,\ -1 \le z \le 1\right\},
\end{aligned}$$

with traces

$$\begin{aligned}
S_1 &= F_1 \cap F_2 = \left\{(x,y,z) \in \mathbb{R}^3 : -1 \le x \le 1/2,\ y = 0,\ z = 0\right\}, \\
S_2 &= F_1 \cap F_3 = \left\{(x,y,z) \in \mathbb{R}^3 : x = -1/2,\ -1 \le y \le 1,\ z = 0\right\}, \\
S_3 &= F_2 \cap F_3 = \left\{(x,y,z) \in \mathbb{R}^3 : x = -1/2,\ y = 0,\ -1 \le z \le 1\right\}.
\end{aligned}$$

The problem is defined setting non-homogeneous Dirichlet boundary conditions on the whole boundary $\partial\Omega$, and a load term on each fracture in such a way that the exact solution is given by:

$$\begin{aligned}
H_1(x,y) &= \frac{1}{10}\left(-x - \frac{1}{2}\right)\left(8xy\left(x^2+y^2\right)\operatorname{arctan2}(y,x) + x^3\right), \\
H_2(x,z) &= \frac{1}{10}\left(-x - \frac{1}{2}\right)x^3 - \frac{4}{5}\pi\left(-x - \frac{1}{2}\right)x^3\,|z|, \\
H_3(y,z) &= (y-1)y(y+1)(z-1)z,
\end{aligned}$$

where $\operatorname{arctan2}(y,x)$ is the four quadrant inverse tangent function with 2 arguments, that returns the appropriate quadrant of the computed angle y/x. Note that since $H_1, H_2 \notin C^1$, a net flux is expected between F_1 and F_2.

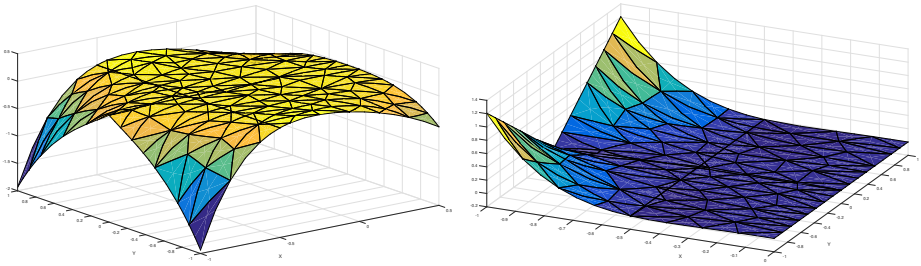

Figure 5: Benchmark problem: computed hydraulic head on fractures F_1 (left) and F_2 (right).

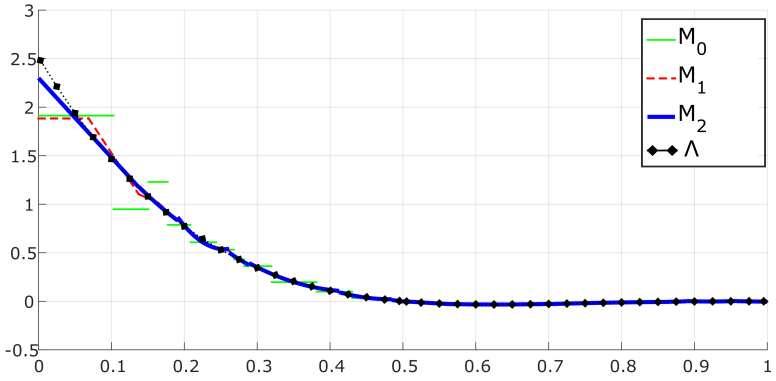

Figure 6: Benchmark problem: computed and exact fluxes

The computed solutions obtained for the hydraulic head on such fractures are shown in Figure 5. Fluxes exchanged between F_1 and F_2, computed with all three considered choices for the mortar bases are shown in Figure 6, where they are compared with the exact one.

In order to present convergence results, we remark that since the values of the discrete solution are not explicitly known inside the elements but only on the set of DOFs, the errors are computed by projecting the discrete solution on the space of polynomials of degree k, as is the usual procedure with the VEM [31]:

$$\left(Err^H_{\mathrm{L}^2}\right)^2 = \sum_{E\in\mathcal{T}_\delta} \|H - \Pi^\nabla_{E,k} h_E\|^2_{\mathrm{L}^2(E)}\,,$$
$$\left(Err^H_{\mathrm{H}^1}\right)^2 = \sum_{E\in\mathcal{T}_\delta} \|H - \Pi^\nabla_{E,k} h_E\|^2_{\mathrm{H}^1(E)}\,,$$

where $\Pi^\nabla_{E,k}$ is the projection operator of order k as defined in Section 3, H is the exact solution and h_E is the discrete solution restricted to element E. Regarding the errors of approximation of Λ, we measure them on each trace both in $\mathrm{L}^2(S)$ and $\mathrm{H}^{-\frac{1}{2}}(S)$ norm; for practical computational issues, we approximate this latter

		h		λ on S_1	
VEM order	Mortar basis	L^2 Norm	H^1 Norm	L^2 Norm	$H^{-\frac{1}{2}}$ Norm
1	M_0	1.00 (1)	0.50 (0.5)	1.19	1.79
1	M_1	1.00 (1)	0.50 (0.5)	1.26	1.87
2	M_0	1.38 (1.5)	0.91 (1)	0.98	1.54
2	M_1	1.50 (1.5)	1.01 (1)	1.54	2.05
2	M_2	1.51 (1.5)	1.01 (1)	2.45	3.02

Table 1: Benchmark problem: convergence rates for several VEM orders and Mortar bases. The numbers in parentheses indicate the expected rates.

norm with a weighted $L^2(S)$ norm:

$$\left(Err^{\Lambda}_{L^2}\right)^2 = \sum_{S\in\mathcal{S}}\sum_{e\subset S} \|\Lambda-\lambda\|^2_e\,,$$

$$\left(Err^{\Lambda}_{H^{-\frac{1}{2}}}\right)^2 = \sum_{S\in\mathcal{S}}\sum_{e\subset S} |e|\,\|\Lambda-\lambda\|^2_e\,.$$

In Figure 7, focusing on fracture F_1, we present the convergence curves for different combinations of the order k for the VEM space and of the type of Mortar basis. Namely, in the left column we report the behavior of the errors $Err^H_{L^2}$ and $Err^H_{H^1}$ (labeled by L^2 and H^1, respectively); the errors are plot versus the total number of h-DOFs on the fracture. In the right column we report the errors $Err^{\Lambda}_{L^2}$ and $Err^{\Lambda}_{H^{-\frac{1}{2}}}$ (labeled by L^2 and $H^{-1/2}$, respectively); here, the errors are plot versus the number of λ-DOFs on the traces of F_1.

Finally, Table 1 reports, for all the analysed cases, the computed convergence rates with respect to the number of DOFs. Namely, we report the computed rates of convergence for h with respect to the h-DOFs (the expected values being reported in parentheses); note the very good agreement between the computed and the expected rates, except for the case $k = 2$ and M_0, in which the low order of the mortar basis slows down the rate of convergence for the hydraulic head. Focusing on trace S_1, we also report the computed rates of convergence for λ with respect to the number of λ-DOFs. The rates of convergence for the λ-errors with respect to the number of h-DOFs, not listed here, are approximately one half of the reported values; this is in agreement with the fact that the number of λ-DOFs scales as the square root of the number of h-DOFs.

6.2. Complex networks

In this section we present results obtained on more complex networks. The first one, DFN36, consists of 36 fractures. The geometry of the DFN is depicted in Figure 8, from which the geometrical complexity of the domain can be seen. A non-homogeneous constant Neumann boundary condition ($H^N = 100$) has been set on one fracture (called source fracture), and a homogeneous Dirichlet boundary condition has been set on another fracture (sink fracture). Homogeneous Neumann boundary conditions on the remaining part of the boundary isolate all the other fractures from the surrounding medium.

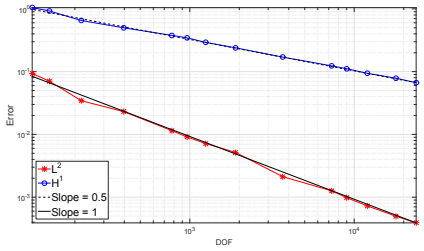

(a) Order 1 - M_0 - Error in h

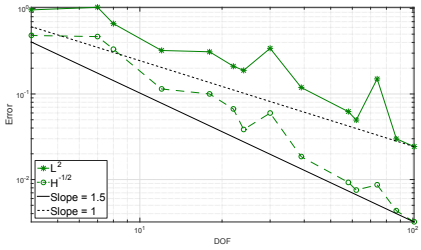

(b) $k = 1$ - Basis M_0 - Error in λ

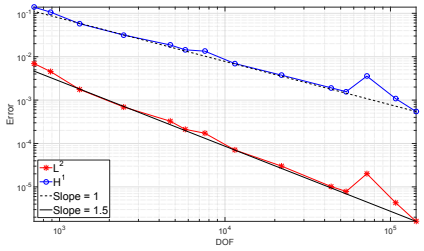

(c) $k = 2$ - Basis M_0 - Error in h

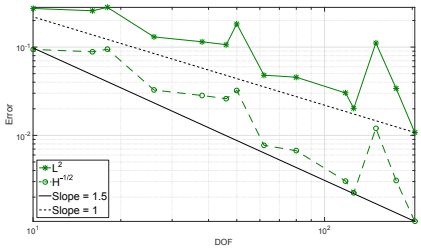

(d) $k = 2$ - Basis M_0 - Error in λ

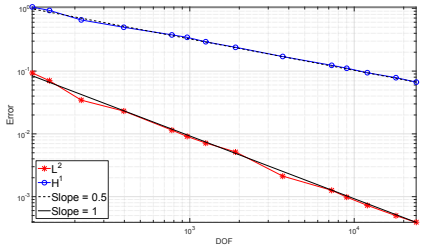

(e) $k = 1$ - Basis M_1 - Error in h

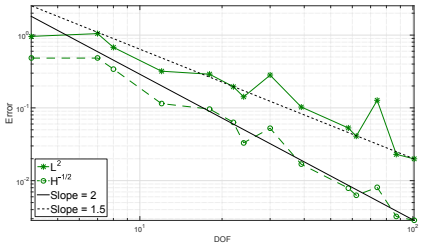

(f) $k = 1$ - Basis M_1 - Error in λ

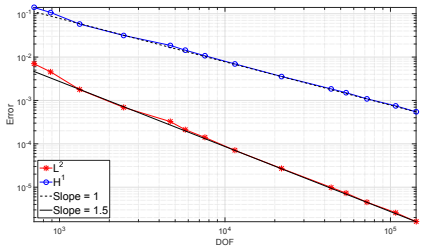

(g) $k = 2$ - Basis M_1 - Error in h

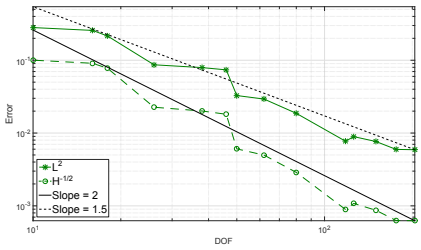

(h) $k = 2$ - Basis M_1 - Error in λ

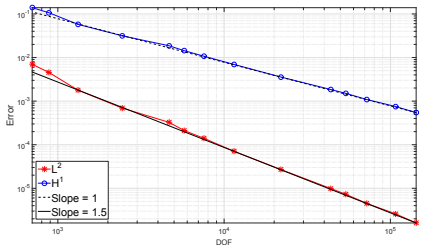

(i) $k = 2$ - Basis M_2 - Error in h

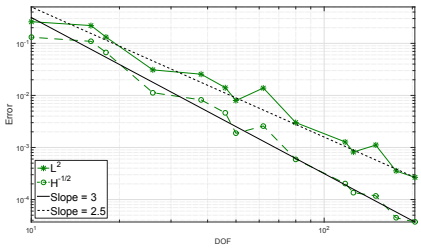

(j) $k = 2$ - Basis M_2 - Error in λ

Figure 7: Benchmark problem: convergence curves measured on fracture F_1

Figure 8: DFN36: geometry of the network and computed hydraulic head (as a scale of colours)

The plots in Figure 9 report the computed total net fluxes exchanged by the source and sink fracture versus the number of DOFs on traces (logaritmic x-scale), for VEM of order $k = 1, 2$ and 3, and mortar bases M_0, M_1 and M_2. The value Δ reported is the difference between the two curves and is an indication of the global conservation state of the method in the whole DFN. Results show the tendency to approximate the expected values and we note that, interestingly, almost no difference in flux values is appreciated for different choices of mortar bases. As a further quality indicator for the obtained solution, we introduce a measure of the error of the jump of the hydraulic head on traces. Namely, we set

$$E_h = \sum_{S \in \mathcal{S}} \| [\![h]\!]_S \|^2_{\mathrm{L}^2(S)} .$$

The computed values are shown in Figure 10 for VEM of order $k = 1, 2$ and 3, using the basis M_1. For all orders, a decrease in this parameter was observed with increasing number of DOFs as expected, but interestingly, with a similar rate. Since the defined quantity does not constitute a norm, no further conclusions about convergence can be drawn.

As a second example, a 134 fracture network is proposed (DFN134, Figure 11). As far as geometrical complexities are concerned, this DFN is far more challenging than DFN36, as it exhibits several critical features: very small angles at trace intersections (thus challenging the shape regularity of the elements stated by Assumption 1 and discussed in Remark 5.1), almost parallel traces, large variation of trace lengths and fracture sizes. Three fractures were chosen as

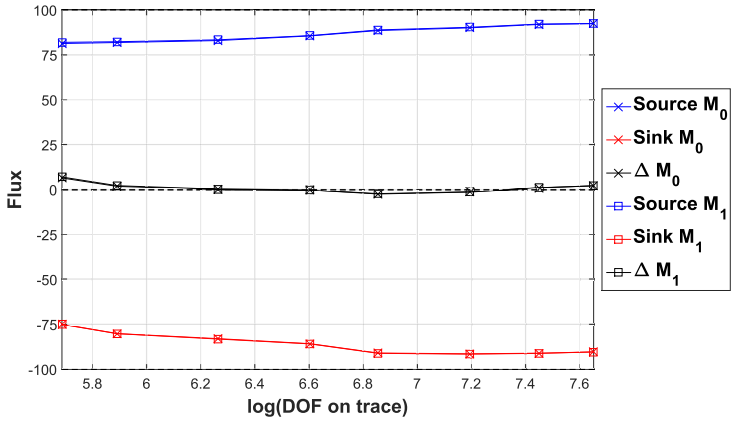

(a) $k = 1$

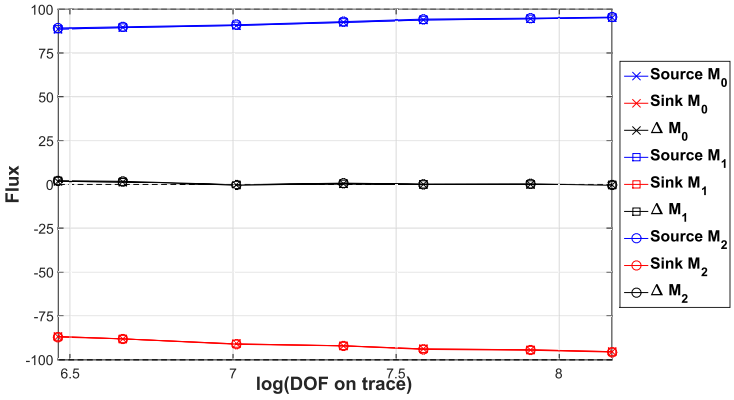

(b) $k = 2$

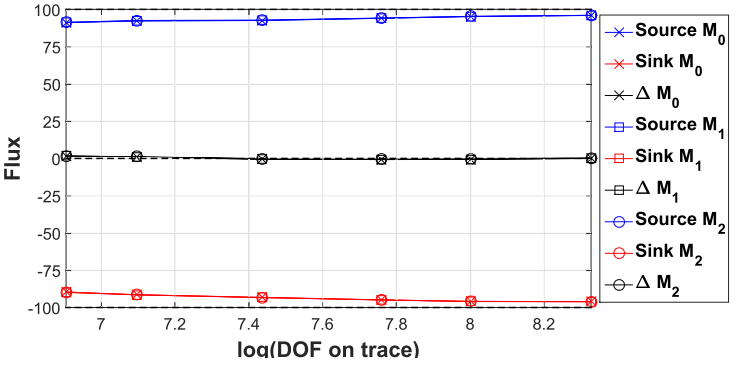

(c) $k = 3$

Figure 9: DFN36: flux results

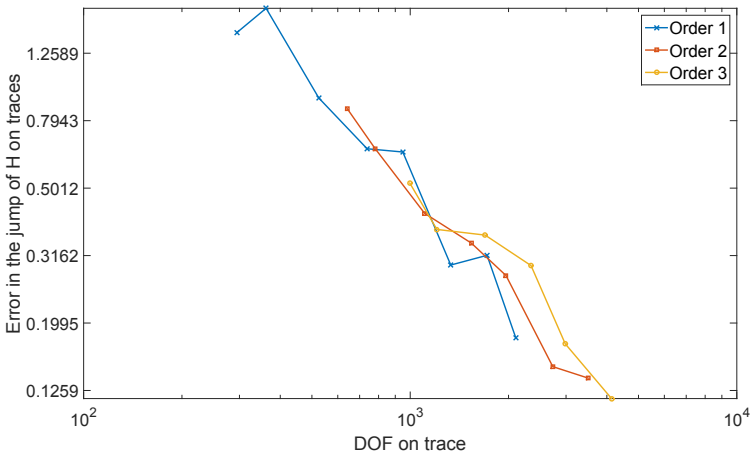

Figure 10: DFN36: error in the jump of the hydraulic head on traces

source fractures by imposing non-homogeneous Neumann boundary conditions. A fourth fracture was set as sink fracture, and on one of its edges a homogeneous Dirichlet boundary conditions was set. Homogeneous Neumann conditions were imposed on all the remaining components of the boundary.

In Figure 12 we report some data for a particularly intricate fracture, where the problem has been solved using VEM of order $k = 2$ and the M_1 basis. The VEM mesh is presented (top left figure), as well as the affine interpolation of the computed hydraulic head solution (bottom left) and the corresponding velocity field obtained from the gradients of the computed hydraulic head (top right figure). From the detail reported in the bottom right figure, it can be seen how elements of order 2 allow for a better representation of the change in slope between close traces thanks to the added DOFs in the midpoints of each of the edges.

7. Conclusions

We have introduced a new approach for flow simulations in Discrete Fracture Networks. The key feature is given by its capability to work with arbitrary (good quality) meshes generated on the fractures. Taking advantage of the versatility of the Virtual Element Method in handling polygonal meshes, each arbitrary mesh is easily modified in such a way that local conformity of the meshes is obtained for almost any trace disposition. Using the hybrid formulation of the Mortar method, only "weak" continuity is required for the hydraulic head along the intersections between fractures.

The main advantage of the approach presented here, with respect to the method proposed in [23], is that, besides the computation of the hydraulic head, the present approach allows for a direct approximation of the flux on

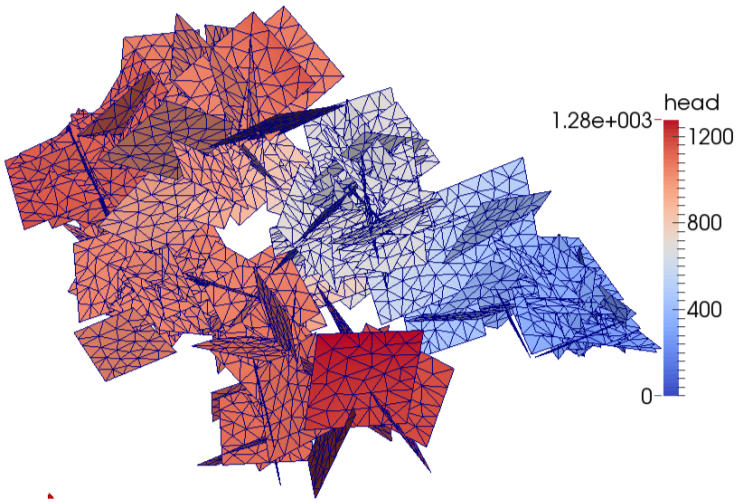

Figure 11: DFN134: geometry of the network and computed hydraulic head (as a scale of colours)

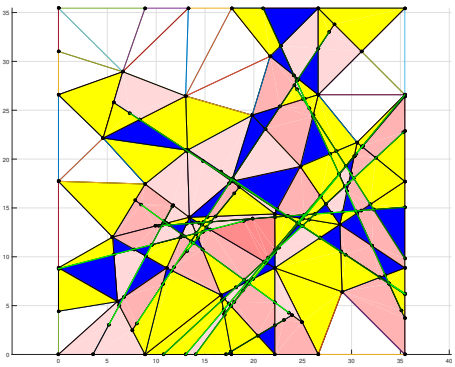

(a) Mesh

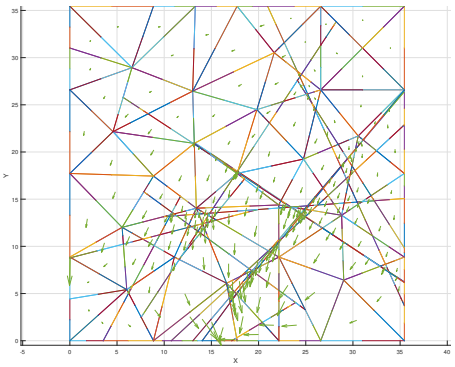

(b) Velocity field solution

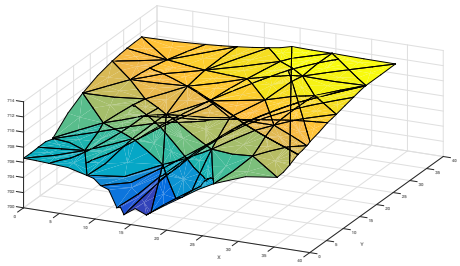

(c) Hydraulic head solution

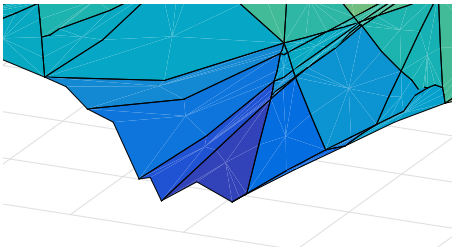

(d) Detail of hydraulic head solution

Figure 12: DFN134: a selected fracture

each trace, whereas in [23] the flux exchange is derived from the values of the hydraulic head.

The validity of the approach proposed is supported by numerical experiments, showing optimal convergence for the primal variable; furthermore, the behaviour of the method is quite satisfactory also when it is applied to DFNs with complex geometry.

Future developments include the extension to more complex flow models and in particular to the case of non-constant transmissivity values. Furthermore, we aim at investigating a possible parallel implementation, which is recommended for tackling large scale DFNs for realistic underground flow simulations.

Appendix A. Proof of Theorem 4.1

This Appendix is devoted to the proof of Theorem 4.1. The proof follows the lines of proofs of [36, Theorem 3] and [24, Theorem 3.1]. We first prove the following preliminary result, which extends Poincaré's inequality to a DFN.

Lemma A.1. *Let* $\tilde{W} = \left\{ v \in V \colon \int_S [\![v]\!] = 0 \quad \forall S \in \mathcal{S} \right\}$. *Then*

$$\exists C_\Omega > 0 \colon \forall w \in \tilde{W} \qquad \left(\sum_{i=1}^{N} \| w \|^2_{\mathrm{L}^2(F_i)} \right)^{\frac{1}{2}} \leq C_\Omega \, |\!|\!| \, w \, |\!|\!| \tag{A.1}$$

Proof. First, notice that $|\!|\!| \cdot |\!|\!|$ is a norm on $\tilde{W}$ (see Proposition 4.1), thus the right hand side of (A.1) does not vanish, unless w is identically zero. By contradiction, suppose

$$\forall C > 0, \, \exists w_C \in \tilde{W} \colon \| \, w_C \, \|_\Omega := \left(\sum_{i=1}^{N} \| w_C \|^2_{\mathrm{L}^2(F_i)} \right)^{\frac{1}{2}} > C \, |\!|\!| \, w_C \, |\!|\!| \, ,$$

then it is possible to build a sequence $w_k \in \tilde{W}$, $k \in \mathbb{N}$, of functions such that $\| \, w_k \, \|_\Omega > k \, |\!|\!| \, w_k \, |\!|\!|$ and, without loss of generality, suppose that $\| \, w_k \, \|_\Omega = 1$ for all k. Then, since $\| \, w_k \, \|_{\mathrm{H}^1(F_i)}$ is limited for all $i = 1, \ldots, N$, w_k converges weakly in V to a function $w^\star$ up to sub-sequences. Clearly, ∇w_k converges to $\nabla w^\star$ weakly. Then, since

$$0 \leq \| \nabla w_k - \nabla w^\star \|^2_{\mathrm{L}^2(F_i)} = \| \nabla w_k \|^2_{\mathrm{L}^2(F_i)} - 2 (\nabla w_k, \nabla w^\star)_{\mathrm{L}^2(F_i)} + \| \nabla w^\star \|^2_{\mathrm{L}^2(F_i)} \, ,$$

and $\| \, \nabla w_k \, \|_{\mathrm{L}^2(F_i)} < \frac{1}{k}$, taking the limit for $k \to \infty$, it follows that $\| \, \nabla w^\star \, \|_{\mathrm{L}^2(F_i)} = 0$. Then, $w^\star$ is constant on each fracture. By the same arguments used in the proof of Proposition 4.1, it follows that $w^\star$ must be the null function. Moreover, since $\mathrm{H}^1(F_i)$ is compactly embedded in $\mathrm{L}^2(F_i)$, w_k converges strongly to $w^\star$ in $\mathrm{L}^2(F_i)$, for all $i = 1, \ldots, N$. Since $\| \, w_k \, \|_{\mathrm{L}^2(F_i)} \overset{k \to \infty}{\longrightarrow} \| \, w^\star \, \|_{\mathrm{L}^2(F_i)}$ for all $i = 1, \ldots, N$, we obtain $\| \, w^\star \, \|_\Omega = 1$, which is a contradiction. □

We can now prove the a priori error estimate.

Proof of Theorem 4.1. Let $h_l \in W_\delta^D$ be the a-orthogonal projection of $H \in V^D$ over W_δ^D, such that

$$\forall v_\delta \in W_\delta^D, \qquad a\left(H - h_l, v_\delta\right) = 0\,.$$

Exploiting the properties of the projection, we have

$$\left\|\!\left|\, H - h \,\right|\!\right\|^2 = \left\|\!\left|\, H - h_l \,\right|\!\right\|^2 + \left\|\!\left|\, h_l - h \,\right|\!\right\|^2 = \left(\inf_{v_\delta \in W_\delta^D} \left\|\!\left|\, H - v_\delta \,\right|\!\right\| \right)^2 + \left\|\!\left|\, h_l - h \,\right|\!\right\|^2 .$$

As far as the second term is concerned, recalling (19) we have

$$\alpha_* \left\|\!\left|\, h_l - h \,\right|\!\right\|^2 = \alpha_* a(h_l - h, h_l - h) \leq a_\delta(h_l - h, h_l - h)\,.$$

By using the problem definitions (12) and (24), and introducing an arbitrary $p \in \mathbb{P}_k^D$, for which (17) holds, we have

$$\begin{aligned}
a_\delta\left(h_l - h, h_l - h\right) &= a_\delta\left(h_l - p, h_l - h\right) + a_\delta\left(p, h_l - h\right) - a_\delta\left(h, h_l - h\right) \\
&= a_\delta\left(h_l - p, h_l - h\right) + a(p, h_l - h) - \left(f, h_l - h\right)_\delta \\
&\quad + b\left(h_l - h, \lambda\right) - \left(H^N, h_l - h\right)_{\Gamma^N} \\
&= a_\delta\left(h_l - p, h_l - h\right) + a(p - H, h_l - h) + a(H, h_l - h) \\
&\quad - \left(f, h_l - h\right)_\delta + b\left(h_l - h, \lambda\right) - \left(H^N, h_l - h\right)_{\Gamma^N} \\
&= a_\delta\left(h_l - p, h_l - h\right) + a(p - H, h_l - h) \\
&\quad - \left(f, h_l - h\right)_\delta + \left(f, h_l - h\right) - b\left(h_l - h, \Lambda\right) ,
\end{aligned}$$

where we have used that $b\left(h_l - h, \lambda\right) = 0$ because $h_l - h \in W_\delta$. Introducing $\mathscr{F}$, $\mathscr{F}_\delta$ and a generical $\psi_\delta \in M_\delta$, since $b\left(h_l - h, \psi_\delta\right) = 0$ we have

$$\begin{aligned}
a_\delta\left(h_l - h, h_l - h\right) &= a_\delta\left(h_l - p, h_l - h\right) + a(p - H, h_l - h) - b\left(h_l - h, \Lambda\right) \\
&\quad + {}_{V'}\langle \mathscr{F} - \mathscr{F}_\delta, h_l - h \rangle_V \\
&\leq \left(\alpha^* \left\|\!\left|\, h_l - p \,\right|\!\right\| + \left\|\!\left|\, H - p \,\right|\!\right\| + \frac{b\left(h_l - h, \Lambda - \psi_\delta\right)}{\left\|\!\left|\, h_l - h \,\right|\!\right\|} \right) \left\|\!\left|\, h_l - h \,\right|\!\right\| \\
&\quad + \left\| \mathscr{F} - \mathscr{F}_\delta \right\|_{V'} \left\| h_l - h \right\|_V \\
&\leq \left(\alpha^* \left\|\!\left|\, h_l - p \,\right|\!\right\| + \left\|\!\left|\, H - p \,\right|\!\right\| + \frac{b\left(h_l - h, \Lambda - \psi_\delta\right)}{\left\|\!\left|\, h_l - h \,\right|\!\right\|} \right. \\
&\quad \left. + \left(1 + C_\Omega\right) \left\| \mathscr{F} - \mathscr{F}_\delta \right\|_{V'} \right) \left\|\!\left|\, h_l - h \,\right|\!\right\| ,
\end{aligned}$$

where in the last step inequality (A.1) has been used (see (13) for the definition of the V-norm). The proof of (30) is thus completed using the triangle inequality and suitably taking the supremums and infimums.

In order to prove (31), let us consider an arbitrary $\psi_\delta \in M_\delta$. By applying

(27), (12) and (24) we get:

$$\beta \| \psi_\delta - \lambda \|_M \leq \sup_{v_\delta \in V_\delta} \frac{b(v_\delta, \psi_\delta - \lambda)}{\| v_\delta \|_V} = \sup_{v_\delta \in V_\delta} \frac{b(v_\delta, \Lambda - \lambda) + b(v_\delta, \psi_\delta - \Lambda)}{\| v_\delta \|_V}$$
$$= \sup_{v_\delta \in V_\delta} \frac{a_\delta(h, v_\delta) - (f, v_\delta)_\delta - a(H, v_\delta) + (f, v_\delta) + b(v_\delta, \psi_\delta - \Lambda)}{\| v_\delta \|_V}.$$

Next, introducing an arbitrary $p \in \mathbb{P}_k^D(\Omega)$, by (17) we get

$$\begin{aligned}
\beta \| \psi_\delta - \lambda \|_M &\leq \sup_{v_\delta \in V_\delta} \| v_\delta \|_V^{-1} \Big[a_\delta(h - p, v_\delta) + a(p - H, v_\delta) \\
&\qquad + {}_{V'}\langle \mathscr{F} - \mathscr{F}_\delta, v_\delta \rangle_V + b(v_\delta, \psi_\delta - \Lambda) \Big] \\
&\leq \sup_{v_\delta \in V_\delta} \| v_\delta \|_V^{-1} \left[\sqrt{a_\delta(h - p, h - p)} \sqrt{a_\delta(v_\delta, v_\delta)} \right] + |\!|\!| H - p |\!|\!| \\
&\quad + \| \mathscr{F} - \mathscr{F}_\delta \|_{V'} + \| \Lambda - \psi_\delta \|_M \\
&\leq \sqrt{\alpha^*} |\!|\!| h - p |\!|\!| + |\!|\!| H - p |\!|\!| + \| \mathscr{F} - \mathscr{F}_\delta \|_{V'} + \| \Lambda - \psi_\delta \|_M \\
&\leq \sqrt{\alpha^*} |\!|\!| H - h |\!|\!| + (1 + \sqrt{\alpha^*}) |\!|\!| H - p |\!|\!| + \| \mathscr{F} - \mathscr{F}_\delta \|_{V'} + \\
&\quad + \| \Lambda - \psi_\delta \|_M .
\end{aligned}$$

The proof is concluded by the triangle inequality and taking the infimum over $\mathbb{P}_k^D(\Omega)$. □

References

[1] C. Fidelibus, G. Cammarata, M. Cravero, Hydraulic characterization of fractured rocks. In: Abbie M, Bedford JS (eds) Rock mechanics: new research., Nova Science Publishers Inc., New York, 2009.

[2] J. Bear, A. H.-D. Cheng, Modeling Groundwater Flow and Contaminant Transport, no. 23 in Theory and Applications of Transport in Porous Media, Springer, 2010.

[3] P. M. Adler, Fractures and Fracture Networks, Kluwer Academic, Dordrecht, 1999.

[4] M. C. Cacas, E. Ledoux, G. de Marsily, B. Tillie, A. Barbreau, E. Durand, B. Feuga, P. Peaudecerf, Modeling fracture flow with a stochastic discrete fracture network: calibration and validation: 1. the flow model, Water Resour. Res. 26 (1990) 479–489.

[5] W. S. Dershowitz, C. Fidelibus, Derivation of equivalent pipe networks analogues for three-dimensional discrete fracture networks by the boundary element method, Water Resource Res. 35 (1999) 2685–2691.

[6] B. Nœtinger, N. Jarrige, A quasi steady state method for solving transient Darcy flow in complex 3D fractured networks, Journal of Computational Physics 231 (1) (2012) 23 – 38. doi:http://dx.doi.org/10.1016/j.jcp.2011.08.015.

[7] B. Nœtinger, A quasi steady state method for solving transient Darcy flow in complex 3D fractured networks accounting for matrix to fracture flow, Journal of Computational Physics 283 (2015) 205–223. doi:http://dx.doi.org/10.1016/j.jcp.2014.11.038.

[8] S. Berrone, S. Pieraccini, S. Scialò, A PDE-constrained optimization formulation for discrete fracture network flows, SIAM J. Sci. Comput. 35 (2) (2013) B487–B510. doi:10.1137/120865884.

[9] S. Berrone, S. Pieraccini, S. Scialò, On simulations of discrete fracture network flows with an optimization-based extended finite element method, SIAM J. Sci. Comput. 35 (2) (2013) A908–A935. doi:10.1137/120882883.

[10] S. Berrone, S. Pieraccini, S. Scialò, An optimization approach for large scale simulations of discrete fracture network flows, J. Comput. Phys. 256 (2014) 838–853. doi:10.1016/j.jcp.2013.09.028.

[11] L. Formaggia, P. Antonietti, P. Panfili, A. Scotti, L. Turconi, M. Verani, A. Cominelli, Optimal techniques to simulate flow in fractured reservoir, in: ECMOR XIV-14th European conference on the mathematics of oil recovery, 2014.

[12] J. D. Hyman, C. W. Gable, S. L. Painter, N. Makedonska, Conforming Delaunay triangulation of stochastically generated three dimensional discrete fracture networks: A feature rejection algorithm for meshing strategy, SIAM Journal on Scientific Computing 36 (4) (2014) A1871–A1894.

[13] G. Pichot, J. Erhel, J. de Dreuzy, A mixed hybrid mortar method for solving flow in discrete fracture networks, Applicable Analysis 89 (10) (2010) 1629–1643.

[14] G. Pichot, J. Erhel, J. de Dreuzy, A generalized mixed hybrid mortar method for solving flow in stochastic discrete fracture networks, SIAM Journal on scientific computing 34 (1) (2012) B86–B105.

[15] H. Mustapha, R. Dimitrakopoulos, High-order stochastic simulation of complex spatially distributed natural phenomena, Mathematical Geosciences 42 (5) (2010) 457–485.

[16] S. Berrone, C. Canuto, S. Pieraccini, S. Scialò, Uncertainty quantification in discrete fracture network models: Stochastic fracture transmissivity, Computers & Mathematics with Applications 70 (2015) 603–623.

[17] Z. Huang, X. Yan, J. Yao, A two-phase flow simulation of discrete-fractured media using mimetic finite difference method, Communications in Computational Physics 16 (3).

[18] H. Mustapha, K. Mustapha, A new approach to simulating flow in discrete fracture networks with an optimized mesh, SIAM J. Sci. Comput. 29 (4) (2007) 1439–1459. doi:http://dx.doi.org/10.1137/060653482.

[19] S. Berrone, S. Pieraccini, S. Scialò, F. Vicini, A parallel solver for large scale dfn simulations, SIAM Journal on Scientific Computing 37 (3) (2015) C285–C306.

[20] M. Karimi-Fard, L. J. Durlofsky, Unstructured adaptive mesh refinement for flow in heterogeneous porous media, in: ECMOR XIV-14th European conference on the mathematics of oil recovery, 2014.

[21] J. Jaffré, J. E. Roberts, Modeling flow in porous media with fractures; discrete fracture models with matrix-fracture exchange, Numerical Analysis and Applications 5 (2) (2012) 162–167.

[22] M. F. Benedetto, S. Berrone, S. Pieraccini, S. Scialò, The virtual element method for discrete fracture network simulations, Computer Methods in Applied Mechanics and Engineering 280 (2014) 135 – 156. doi:http://dx.doi.org/10.1016/j.cma.2014.07.016.

[23] M. F. Benedetto, S. Berrone, S. Scialò, A globally conforming method for solving flow in discrete fracture networks using the virtual element method, Finite Elements in Analysis and Design 109 (2016) 23–36.

[24] L. Beirão da Veiga, F. Brezzi, A. Cangiani, G. Manzini, L. D. Marini, A. Russo, Basic principles of virtual element methods, Math. Models Methods Appl. Sci. 23 (1) (2013) 199–214. doi:10.1142/S0218202512500492.

[25] C. Bernardi, Y. Maday, A. T. Patera, A new nonconforming approach to domain decomposition: the mortar element method, in: Nonlinear partial differential equations and their applications. Collège de France Seminar, Vol. XI (Paris, 1989–1991), Vol. 299 of Pitman Res. Notes Math. Ser., Longman Sci. Tech., Harlow, 1994, pp. 13–51.

[26] L. Beirão da Veiga, F. Brezzi, L. D. Marini, A. Russo, The hitchhiker's guide to the virtual element method, Mathematical Models and Methods in Applied Sciences 24 (08) (2014) 1541–1573. doi:10.1142/S021820251440003X.

[27] L. Beirão da Veiga, G. Manzini, A virtual element method with arbitrary regularity, IMA Journal of Numerical Analysis 34 (2) (2014) 759–781. doi:10.1093/imanum/drt018.

[28] B. Ahmad, A. Alsaedi, F. Brezzi, L. D. Marini, A. Russo, Equivalent projectors for virtual element methods, Comput. Math. Appl. 66 (3) (2013) 376–391. doi:10.1016/j.camwa.2013.05.015.

[29] A. Cangiani, G. Manzini, A. Russo, N. Sukumar, Hourglass stabilization and the virtual element method, International Journal for Numerical Methods in Engineering 102 (3-4) (2015) 404–436, nme.4854. doi:10.1002/nme.4854.

[30] B. Ayuso de Dios, K. Lipnikov, G. Manzini, The nonconforming virtual element method, ArXivdoi:arXiv:1405.3741.

[31] L. Beirão da Veiga, F. Brezzi, L. D. Marini, A. Russo, Virtual element methods for general second order elliptic problems on polygonal meshes, arXivdoi:2014arXiv1412.2646B.

[32] K. Lipnikov, G. Manzini, M. Shashkov, Mimetic finite difference method, Journal of Computational Physics 257 (2014) 1163–1227.

[33] L. Beirão da Veiga, K. Lipnikov, G. Manzini, The Mimetic Finite Difference Method for Elliptic Problems, Vol. 11 of Modeling, Simulation & Applications, Springer, 2014.

[34] F. Brezzi, On the existence, uniqueness and approximation of saddle-point problems arising from lagrangian multipliers, Revue française d'automatique, informatique, recherche opérationelle. Analyse numérique 8 (2) (1974) 129–151.

[35] F. B. Belgacem, The mortar finite element method with lagrange multipliers, Numerische Mathematik 84 (2) (1999) 173–197.

[36] P. Raviart, J. Thomas, Primal hybrid finite element methods for 2nd order elliptic equations, Mathematics of computation 31 (138) (1977) 391–413.

[37] B. Wohlmuth, Discretization Methods And Iterative Solvers Based On Domain Decomposition, Springer, 2001.